Shaped Reflector Antenna Analysis by Graphical Processing Methods

J.M. Rius, Mercè Vall-llossera, C. Salazar, A. Cardama*

Abstract—**This paper presents the application of *GRECO* code to obtain the radiation pattern of single reflector antennas. Shaped reflectors with arbitrary geometries are modelled by CAD software. The *GRECO* graphical processing technique [3][4] [5] is used in order to extract the relevant geometrical information from the CAD geometry database. Surface reflection and edge diffraction are respectively analyzed by Physical Optics approximation and Equivalent Edge Currents method.**

I. Introduction

Shaped or conformed reflector antennas show increasing use in applications that require far-field shaping. Physical optics (PO) and equivalent edge currents (EEC) methods have been extensively used for analyzing surface reflection and edge diffraction of electrically large reflectors [7][8][9][10].

The new concept incorporated by GRECO (GRaphical Electromagnetic COmputing) approach [1][2][3][4][5][6] in order to obtain the geometry information required by high-frequency approximations allows the analysis of arbitrarily shaped surfaces and edges. This technique, that was first developed to analyze the Radar Cross Section (RCS) of complex radar targets, offers a very efficient solution for designing, analyzing and optimizing shaped reflector antennas.

As shown in figure 1, the GRECO approach has three main steps: modeling, geometrical pre-processing and electromagnetic computation. The reflector surface and feeding structure are modelled using a Computer Aid Design (CAD) package. The resulting geometry database is processed by the graphics accelerator of a high performance workstation to render an image of the reflector and feeding structure. Graphical processing of the image provides the geometrical information relevant to high-frequency techniques:

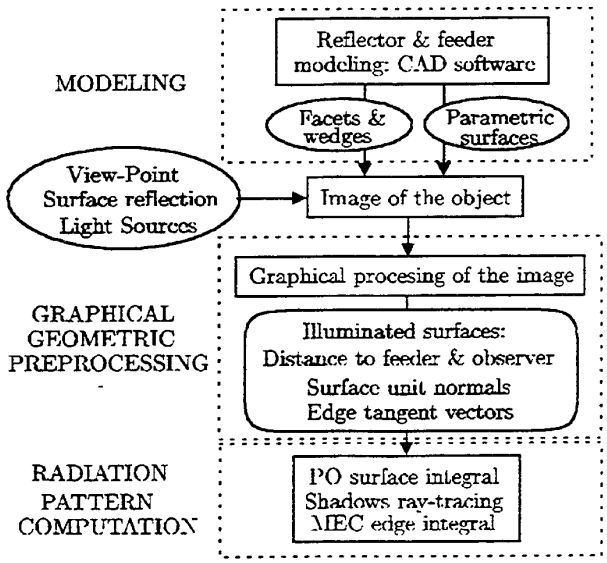

Figure 1 – Block diagram for the GRECO approach. The radiation pattern of a shaped reflector antenna is obtained in three main steps: modeling, geometrical pre-processing and electromagnetic computation.

- The (x, y, z) coordinates and unit normal vector, for each pixel of the reflector surface illuminated by feeder fields.
- The (x, y, z) coordinates and unit tangent vector, for each pixel of the reflector edges illuminated by feeder fields.
- Blockage and shadows in reflector surface due to feeding structure.

The radiation pattern is then computed through PO, EEC and null-field approximations for respectively surface reflection, edge diffraction and blockage. This paper presents the results obtained by PO and EEC methods, while the analysis of blockage and shadows will be presented in a forthcoming paper.

*The authors are with the Dpt. of Signal Theory and Communications, Univ. Politècnica de Catalunya, Gran Capitán s/n, 08034 Barcelona, Spain. This work has been supported by the Spanish Goverment under the grant CYCIT TIC95-0983-C03-03.

II. Modelling

Accurate computation of the radiation pattern of shaped reflector antennas involves the processing of a geometric model of the reflector surface and the blocking structure (figure 2). The main difficulty for PO and EEC analysis of complex geometric models is the computation of surface and line integrals over arbitrarily shaped surfaces and edges, which are modelled by CAD packages using parametric surfaces [11]. These integrals require the knowledge of the unit normal to surfaces and the vector tangent to edges.

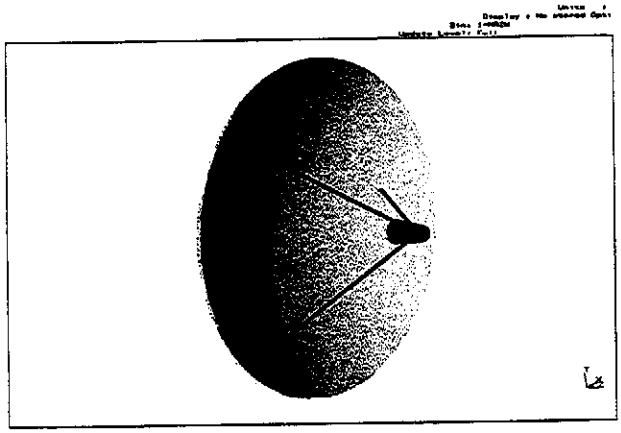

Figure 2 – Symetric parabolic reflector with feeder structure modelled with I-DEAS CAD package.

Parametric surfaces present remarkable features for complex object modeling and high-frequency computations, namely:

- Very good accuracy of the model surface.
- Small number of degrees of freedom, which leads to weak storage requirements and allows optimization of the surface shape.

For that reason computer codes have been recently developed to analyze parametric surface models [12][13][14]. However, the geometrical analysis of these surfaces for the computation of high frequency radiation integrals is complex and requires a large computational cost.

The GRECO technique introduced in [1][3][4][5] for geometrical analysis of the surface is based in the graphical processing of the object image. The graphical processing algorithm is the same for any kind of geometry model, and therefore the GRECO approach takes full profit of the advantages of parametric surface models without increasing the computation run-time.

III. Graphical geometric pre-processing

Hardware graphics accelerators of high-performance workstations are dedicated to render in real time a 3-D visualization of facet and parametric surface geometry models, using realistic lighting and shading. The processing of this image by GRECO technique provides the geometry information necessary for high-frequency scattering computation: coordinates of illuminated surfaces and edges, unit normals and edge tangent vectors. We will use the following convention for 3-D coordinate axis in the object image: (x, y) are the 2-D coordinates along the image, while z is along the observation direction and thus is perpendicular to the xy plane.

A. *Computation of unit normal to surface*

If the scene is rendered using the Phong local illumination model [15], the color of each pixel depends only on the normal to the surface element associated to this pixel and on the location of the observer and light sources. As the position of both the observer and light sources is known, for each pixel of the image it is possible to obtain the normal to the surface from the color information. This technique has been already presented in detail in references [3][4] and can be summarized as follows:

According to Phong illumination model [15], when the surface reflection is diffuse the brightness of a pixel is computed separately for each Red, Green and Blue (R,G,B) color component as proportional to the projection $\hat{n} \cdot \hat{r}_i$ of the unit normal to the surface $\hat{n}$ into the position of the light source $\hat{r}_i$ (figure 3). Therefore, for three light sources of purely red, green and blue colors, respectively located along each one of the three coordinate axis, $\hat{r}_{iR} = \hat{x}$, $\hat{r}_{iG} = \hat{y}$, $\hat{r}_{iB} = \hat{z}$, the three R,G,B color components of a surface element are equal to the (n_x, n_y, n_z) components of the unit normal to the surface. The ambiguity in the sign of (n_x, n_y, n_z) is dealt by separately displaying two different R,G,B images illuminated from opposite directions.

In the object image, the *back-facing* surfaces whose normal points away from the observer half-space are removed by the graphic hardware, and thus only the *front-facing* surfaces are visible. In order to obtain some useful geometric information about non-visible surfaces, two more three-color images are generated in which the unit normals of the model have been reversed and, therefore, the previously *back-facing* surfaces are now visible [5]. The knowledge of the unit normals to those *back-facing* surfaces is required for computing the direction of reflector edges and for detecting shadows produced by the feeder supporting struts.

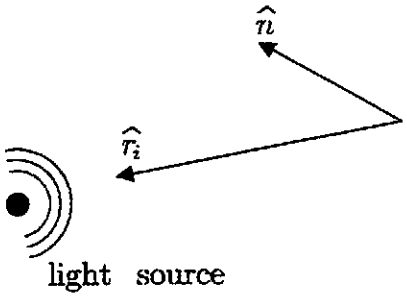

Figure 3 – The color of the surface is obtained as $\hat{n} \cdot \hat{r}_i$, where $\hat{n}$ is the normal to the surface and $\hat{r}_i$ the position of the light source.

B. Computation of radius of curvature

The radius of curvature of the surface in the xz and yz planes can be computed from the variation of the unit normal components n_x and n_y, respectively. Figure 4 shows the procedure to compute the radius of curvature R_x in the xz plane. The procedure for obtaining the radius of curvature in the zy plane, R_y, is analogous. The result is [5]:

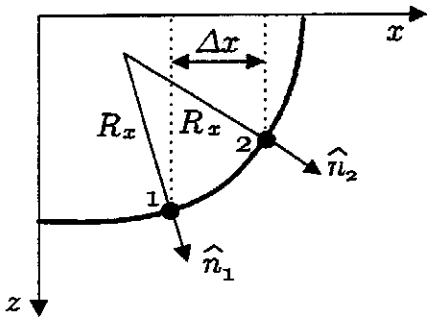

Figure 4 – Computation of the radius of curvature of the surface defined by two adjacent pixels in the xz plane, $R_x = \Delta x / (n_{2x} - n_{1x})$.

$$\frac{1}{R_x} = \frac{n_{2x} - n_{1x}}{\Delta x} \;,\; \frac{1}{R_y} = \frac{n_{2y} - n_{1y}}{\Delta y} \qquad (1)$$

In general, these radius of curvature are not equal to the principal radius of curvature of the surface, and thus cannot be used to compute Geometrical Optics approximation.

C. Edge detection

Edges are detected when any of the radius of curvature (1) defined by two contiguous pixels is smaller than a given threshold, as shown in figure 5.

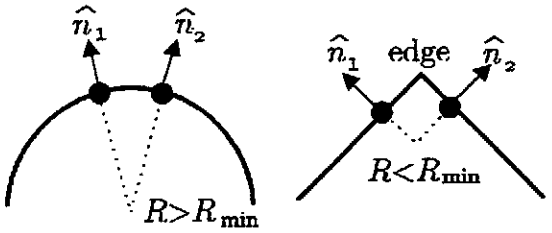

Figure 5 – Edge detection. If the radius of curvature corresponding to two adjacent pixels is less than R_{min} , then there is an edge between these two pixels.

That kind of discontinuities in the unit normal components can also be due to surface eclipses, but that situation is easily discriminated because in that case there is a discontinuity in the z coordinate.

Figure 6 shows the angles that define the orientation of a wedge. The direction of observation $\hat{r}$ is perpendicular to the xy plane and thus $\hat{r}$ is along z axis, $\hat{r} = \hat{z}$. The position of light source $\hat{r}_i$ and the incidence angles ϕ_i, θ_i have been removed for clarity. The wedge orientation angles must be obtained as follows in order to compute the diffraction coefficients for the EEC method:

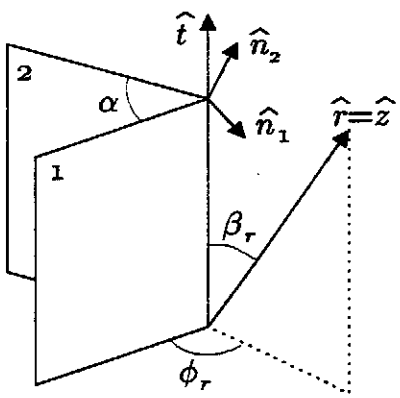

Figure 6 – Wedge geometry.

$$\begin{aligned}
\alpha &= \arccos(-\hat{n}_1 \cdot \hat{n}_2) \\
\hat{t} &= \frac{\hat{n}_1 \times \hat{n}_2}{\sin\alpha} \\
\cos\beta_i &= \hat{t} \cdot \hat{r}_i \\
\cos\beta_r &= \hat{t} \cdot \hat{r} = t_z \\
\sin\phi_i &= \frac{\hat{n}_1 \cdot \hat{r}_i}{\sin\beta_i} \\
\sin\phi_r &= \frac{\hat{n}_1 \cdot \hat{r}}{\sin\beta_r} = \frac{n_{1z}}{\sin\beta_r}
\end{aligned} \qquad (2)$$

When only one face of the wedge is visible, then the other face is a *back-facing* surface and its unit normal

can be obtained from the images with the unit normals reversed. When the unit normals $\hat{n}_1$ and $\hat{n}_2$ are parallel, for example in the edges of most reflectors, we cannot use (2) to compute the edge direction $\hat{t}$. In that case, a special processing of the edge is required in order to obtain the correct value of $\hat{t}$.

IV. Radiation Pattern Computation

Electromagnetic computing, the third main step of GRECO, uses as input the geometry information about the illuminated surfaces and edges obtained by the graphical geometric pre-processing. The most remarkable feature of the GRECO approach is that high-frequency scattering computation is implemented in a way completely independent on the reflector geometry or the kind of geometry model used by the CAD package. The graphical processing technique introduces discretization errors in addition to those inherent to high-frequency approximations. The study of these discretization errors is addressed in [16].

This paper presents the implementation of Physical Optics (PO) and Equivalent Edge Currents (EEC) approximations to analyze surface reflection and edge diffraction. The analysis of blockage by null-field approximation will be addressed in a forthcoming paper.

A. *Physical Optics*

According to Physical Optics theory, the far-field scattered by an electrically large surface can be approximated by

$$\vec{E} = jk\eta \frac{e^{-jkr}}{4\pi r} \hat{r} \times \left(\hat{r} \times \int\int_{\sigma} 2\, \hat{n} \times \vec{H}^i\, e^{\,jk\, \hat{r}\cdot\vec{r}'} ds' \right) \tag{3}$$

where k is the wavenumber, η the wave impedance of free-space, $\hat{n}$ the unit normal to surface, $\vec{H}^i$ the magnetic field incident over a surface element at $\vec{r}'$ and $\hat{r}$ the direction of observation. The surface integral extends along the region σ illuminated by the incident field. Note that the scattered field depends only on the local geometry of σ (unit normal $\hat{n}$ and position $\vec{r}'$) and the incident field $\vec{H}^i$. Local geometry information is obtained from the geometrical pre-processing part of GRECO, while the incident field is obtained from the feeder radiation pattern and its position, orientation and polarization. Feeder radiation patterns, measured or computed, are stored in a feeder library, while the feeder position, orientation and polarization are accounted through a coordinate transformation using Eulerian angles [17].

The procedure for computing the radiation pattern from PO integral (3) is not presented in detail since it is well-known and can be found, for example, in references [7] and [8]. The PO integral (3) is computed numerically by Gauss quadrature. The number of quadrature samples is obtained as follows: by a fast scan of the reflector surface we obtain the path difference Δr between the maximum and minimum reflected ray-paths from the feeder to the observer. Since the magnitude of the integrand usually varies slowly, the required number of samples is determined mainly by the path difference Δr. A sampling density of n samples per wavelength results in a total number of quadrature samples along each direction of integration equal to $n\,(2\Delta r)\,/\lambda$, if the reflector is symmetrical in this direction. Accurate results are obtained by this procedure if the reflector shape is smooth, which is the case for most shaped reflector antennas.

B. *Equivalent Edge Currents*

The far-field scattered by edges is approximated by the field radiated by filamentary electric and magnetic currents located along the edge [10]:

$$\begin{aligned} \vec{E}^r \;=\; & \frac{e^{-jkr}}{4\pi r} E_0 \int_{\ell} \left[D_{je} \left(\hat{e}_i \cdot \hat{t}\right) \hat{r} \times \left(\hat{r} \times \hat{t}\right) \right. \\ & + D_{jh} \left(\hat{h}_i \cdot \hat{t}\right) \hat{r} \times \left(\hat{r} \times \hat{t}\right) \\ & \left. + D_{mh} \left(\hat{h}_i \cdot \hat{t}\right) \left(\hat{r} \times \hat{t}\right) \right] \; e^{jk(\hat{r}+\hat{r}_i)\cdot\vec{r}'} d\ell' \end{aligned} \tag{4}$$

where $\hat{t}$ is the unit vector tangent to the edge. The magnitude of the incident electric field is E_0 and the polarization of incident electric and magnetic fields is respectively $\hat{e}_i$ and $\hat{h}_i$. The line integral extends along the edges ℓ illuminated by the incident field. Coefficients D_{je} and D_{jh} are the directivity patterns of the equivalent electric edge currents induced by the electric and magnetic incident fields, respectively, while D_{mh} is the directivity pattern of the equivalent magnetic edge current induced by the magnetic incident field. These coefficients are known as Incremental Length Diffraction Coefficients (ILDC). There are in the literature different formulations for these coefficients, valid for different regions of observation and showing different singularities. For planar wedges, $\alpha = 0$, we have used Ando's ILDC [9] [10]:

$$\begin{aligned} D_{je} &= 4 \frac{\sin\frac{\phi_i}{2}}{\sin^2\beta_i} \frac{\cos\frac{\phi_i}{2} - \sin\frac{\phi}{2}}{\cos\phi_i + \cos\phi} \\ D_{jh} &= 2 \frac{\cos\beta_i}{\sin^2\beta_i} \\ D_{mh} &= 4 \frac{\cos\frac{\phi}{2}}{\sin^2\beta_i} \frac{\cos\frac{\phi_i}{2} - \sin\frac{\phi}{2}}{\cos\phi_i + \cos\phi} \end{aligned} \tag{5}$$

where β and ϕ angles are defined in figure 6. Unlike other more complex ILDC formulations, Ando's ILDC are valid only for observation in the Keller cone, where $\beta_r = \pi - \beta_i$, corresponding to specular diffraction. Usual reflector shapes have edge specular points for all directions of observation, that produce the main contribution to the line integral (4). Therefore, the use of ILDC valid only on the Keller cone leads to a very good trade-off between simplicity and accuracy.

V. Results

The graphical processing approach for implementation of high-frequency approximations will be compared with standard and analytical computation of PO (3) and EEC (4) integrals. A Hewlett-Packard HP-735 workstation with CRX-48Z graphics accelerator has been used for obtaining graphical processing results.

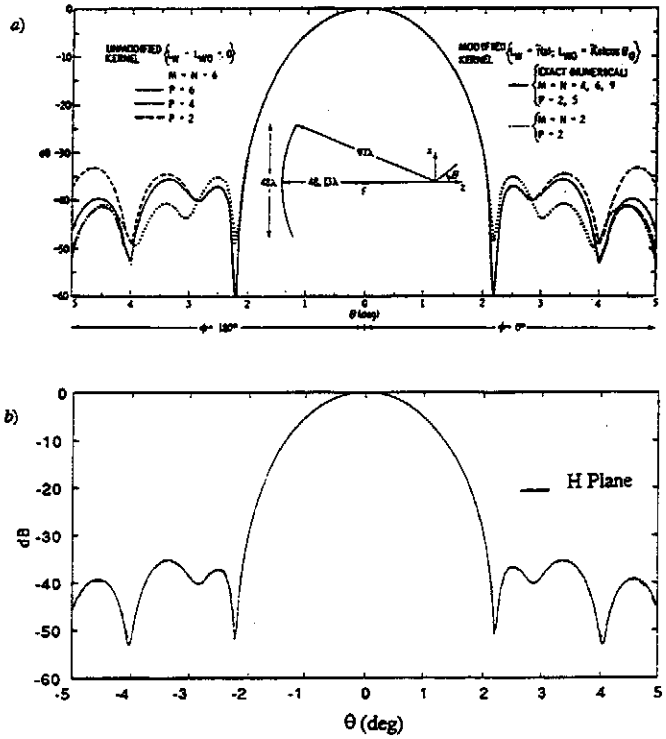

Figure 7 – Radiation pattern of a spherical reflector. Radius of spherical surface is 97λ, aperture diameter is 48λ and distance from reflector center to feeder is 48.13λ. Feeder radiation pattern is axially symmetrical with linear polarization and reflector edge taper equal to -18.5 dB. Top graph (a) shows the results of reference [8], solid line corresponding to exact numerical computation of PO surface integral. Bottom graph (b) shows results of GRECO graphical processing approach.

Figure 7 shows the radiation pattern of a spherical reflector. Radius of spherical surface is 97λ, aperture diameter is 48λ and distance from reflector center to feeder is 48.13λ. Feeder radiation pattern is axially symmetrical with linear polarization,

$$\vec{E} = \cos\phi_s \cos^q \theta_s \hat{\theta}_s + \sin\phi_s \cos^q \theta_s \hat{\phi}_s \qquad (6)$$

where $q = 17.0933$. ϕ_s, θ_s are the spherical angles in the feeder coordinate system, which has origin at the feeder location and z_s axis pointing to the center of the reflector. Resulting reflector edge taper is -18.5 dB.

Top graph (a) shows the results of reference [8], solid line corresponding to exact numerical computation of PO surface integral. Bottom graph (b) shows results of GRECO graphical processing approach. The agreement with exact PO computation is excellent. The CPU time spent in the surface integral computation was 1.55 seconds, using 31 Gaussian quadrature samples along each direction.

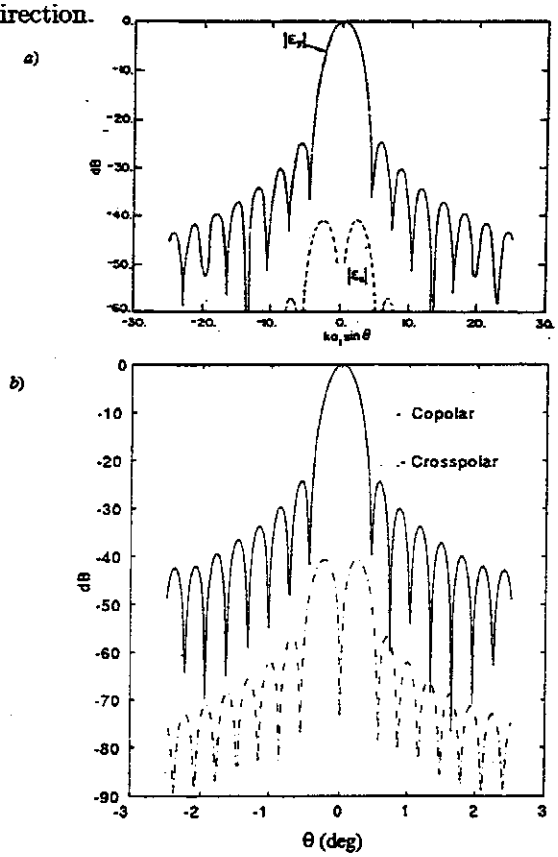

Figure 8 – Radiation pattern of a offset parabolic reflector. Diameter of parent paraboloid is 4533.33λ, reflector aperture diameter is 1866.67λ and focal distance is 4533.33λ. Feeder pattern is again axially symmetrical with linear polarization (6) and edge taper -10 dB. Top graph (a) shows results of standard PO computation, reference [7], for copolar (solid line) and crosspolar (dashed line) polarizations. Bottom graph (b) shows results of GRECO graphical processing approach.

Results obtained for a very large offset parabolic

reflector are shown in figure 8. Diameter of parent paraboloid is 4533.33λ, reflector aperture diameter is 1866.67λ and focal distance is 4533.33λ. Feeder pattern is again axially symmetrical with linear polarization (6). Now z_s axis points to the intersection of the aperture axis with the paraboloid surface (see figure 2 in [7]). Edge taper is -10 dB, obtained with $q = 56.67$.

Top graph (a) shows results of standard PO computation, reference [7], for copolar (solid line) and crosspolar (dashed line) polarizations. Bottom graph (b) shows results of GRECO graphical processing approach. The agreement is, again, excellent for both polarizations. The CPU time spent in the surface integral computation was 38.9 seconds, using 188 Gaussian quadrature samples along each direction.

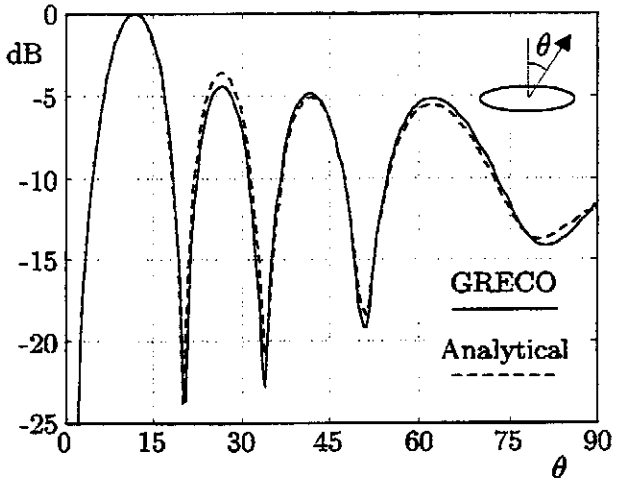

Figure 9 – Edge diffraction pattern of circular flat disk of radius 2.387λ. Analytical computation of edge line integral (4), dashed line, is compared to graphical processing results, solid line. Surface reflection is not considered in order no to mask the edge diffraction contribution. Focal distance is infinite, and thus incident field is a plane wave.

In order to validate the results for edge diffraction, a circular flat disk of radius 2.387λ has been analyzed. Feeder is isotropic and located at an infinite distance along disk axis, producing an incident field equal to a plane wave. Figure 9 compares the analytical computation of edge line integral (4), dashed line, with graphical processing results, solid line. Surface reflection is not considered, in order not to mask the edge diffraction contribution. Graphical processing errors are smaller than 1 dB.

VI. Conclusions

The graphical processing approach (GRECO) for geometrical analysis of arbitrary shapes, previously available only for RCS computation [1] [2][3][4][5], has been applied to the analysis of shaped reflector antennas. GRECO has proved to be a very efficient implementation of physical optics (PO) and equivalent edge currents (EEC) high frequency techniques, showing the following remarkable features:

- Shaped reflector surface is modelled by a CAD package. Parametric surfaces can be used for modelling the reflector and the feeding structure, adjusting very accurately to the real antenna while defining a relatively small number of degrees of freedom.
- Geometrical analysis is done by processing an image of the reflector displayed at a graphical workstation. Geometrical analysis algorithms are therefore independent on the modelling technique used to mathematically describe the reflector surface and edges. This simplifies dramatically the code for electromagnetic computation by PO and EEC methods.
- Simple and fast analysis of arbitrary surfaces and edges allows the interactive design and optimization of shaped reflectors with radiation pattern specifications.

Blockage of feeder and supporting struts is also accounted by null-field approximation. A forthcoming paper will present the graphical processing algorithm for blockage analysis.

References

[1] Juan M. Rius, M. Ferrando, "Real Time Radar Cross Section of Complex Objects by Physical Optics Graphical Processing", *1990 IEEE AP-S International Symposium*, Dallas, Texas, USA, May 7-11, 1990, pp. 1280-1283.

[2] R.A. Shepherd, T.D. Olson and C.S. Liang, "Efficient Signature Estimations in an Advanced Graphics Environment", *1992 IEEE AP-S International Symposium*, Vol. 3, p. 1311.

[3] J.M. Rius, M.Ferrando, L. Jofre, "GRECO: Graphical Electromagnetic Computation for RCS prediction in Real Time", *IEEE Antennas & Propagation Magazine*, vol. 35, no. 2, pp. 7-17, April 1993.

[4] J.M. Rius, M. Ferrando, L. Jofre, "RCS of Complex Radar Targets in real time", *IEEE Transaction on*

Antennas and Propagation, vol. 41, No. 9, pp. 1308-1319, September 1993.

[5] J.M. Rius, M. Vall-llossera, A. Cardama, "Greco: graphical processing methods for high-frequency RCS prediction", *Annales des télécommunications*, vol. 50, no. 5-6, pp. 551-556, May-June 1995.

[6] J.S. Asvestas, "The Physical Optics Integral and Computer Graphics", *IEEE Trans. on Antennas and Propag.*, **43**, no. 12, pp. 1459-1460., December 1995.

[7] R. Mittra, Y. Rahmat- Samii, V. Galindo-Israel, "An Efficient Technique for the Computation of Vector Secondary Pattern of Offset Paraboloid Reflector", *IEEE Transactions on Antennas and Propagation*, vol. 27, no.39, pp. 294-304, May 1979.

[8] Y. Rahmat-Samii, V. Galindo-Israel, "Shaped Reflector Antenna Analysis using the Jacobi-Bessel series". *IEEE Transactions on Antennas and Propagation*, vol. 28, no. 4, pp. 425-435, July 1980.

[9] M. Ando, "Radiation Pattern Analysis of Reflector Antennas", *Electronics and Communications in Japan*, Part. 1, vol. 68, No 4, 1985.

[10] O. Breinbjerg, *"Equivalent Edge Current Analysis of Electromagnetic Scattering by Plane Structures"*, Ph.D. Dissertation, Technical University of Denmark, April 1992

[11] G. Farin, *"Curves and surfaces for computer aided geometric design: a practical guide "*, Academic Press, 1988.

[12] J. Pérez, M.F. Cátedra, "RCS of electrically large target modelled with NURBS surfaces", *Electronic letters*, vol. 28, no. 12, pp. 1119-1121.

[13] J. Pérez, M.F. Cátedra, "Application of Physical Optics to the RCS Computation of Bodies Modeled with NURBS Surfaces", *IEEE Transactions on Antennas and Propagation*, vol. 42, no. 10, pp. 1404-1411, October 1994.

[14] J. Pérez, J.A. Saiz, O.M. Conde, R.P. Torres and M.F. Cátedra, "Analysis of Antennas on Board Arbitrary Structures Modelled by Nurbs Surfaces", *IEEE Transactions on Antennas and Propagation*, vol. 45, no. 6, pp. 1045-1053, June 1997.

[15] J.D. Foley, A. van Dam, S.K. Feiner, J.F. Hughes, *Computer Graphics: Principles and Prcatice*, Addison-Wesley, (1992).

[16] J.M.Rius, D.Burgos, A.Cardama, "Discretization Errors in the Graphical Computation of the Physical Optics Surface Integral", *Applied Computational Electromagnetics Society (ACES) Journal*, Vol. 13, No. 3, pp. 255-263, November 1998.

[17] Y. Rahmat-Samii, "Useful coordinate transformation for antenna applications", *IEEE trans. Antennas Propagation*, vol. 27, pp. 294-304, May 1979.